

STATISTICS OF TURBULENT AND LAMINARIZING FLOW IN A CIRCULAR PIPE WITH A GRADUAL EXPANSION

Nima Moallemi*

School of Engineering
University of British Columbia, Okanagan campus
3333 University Way, Kelowna, BC V1V 1V7
nima.moallemi@gmail.com

Joshua R. Brinkerhoff†

School of Engineering
University of British Columbia, Okanagan campus
3333 University Way, Kelowna, BC V1V 1V7
joshua.brinkerhoff@ubc.ca

ABSTRACT

Direct numerical simulations of turbulent flow in an axisymmetric pipe with a gradual expansion have been performed for a Reynolds number of 5300 based on the inlet pipe diameter and bulk velocity in order to investigate the effect of a gradual expansion on the flow structure, with special focus on the recirculation and laminarization of the flow downstream of the expansion. An annular ribbed turbolator is used in conjunction with a periodic flow mapping approach to produce fully-developed turbulent flow conditions upstream of the gradual expansion. A turbulent free shear layer initiated at the start of the sudden expansion develops from the flow separation and then reattaches to the pipe wall downstream of the expansion. Following reattachment, the turbulent flow laminarizes as the strength and size of vortical structures gradually diminish. The laminarization process is described in terms of the evolution of the Reynolds stress tensor in the turbulent and laminarizing regions, morphometrically in terms of the evolution of coherent vortical structures, and mechanistically through analysis of the budgets of the vorticity transport equation.

INTRODUCTION

Fully developed incompressible turbulent flow through a smooth pipe with a diverging section is a common feature of pipeline networks (Duguet 2015). The increasing pipe diameter reduces the flow Reynolds number and in some cases laminarization of the flow downstream of expansion may occur. Many experimental and numerical investigations have been performed to study the instability mechanism and flow pattern in the context of an axisymmetric sudden expansion. Comparatively fewer works have studied the effect of a gradual expansion on the flow. Peixinho and Besnard (2013) observed transition, localized turbulence, and laminarization of the flow in experiments of slowly diverging pipes. Recently, Selvam, Peixinho, and Willis (2015) performed direct numerical simulation for purely laminar flow in a gradual expansion

between two pipes with a constant finite-amplitude perturbation applied to simulate experimental imperfections. They describe the development of shear layer instability, bifurcation phenomena, and localised turbulence in the gradual expansion for laminar inflow conditions. The goal of the present investigation is to extend their analysis to turbulent inflow conditions in order to identify how the impact of the gradual expansion on the statistics and evolution of coherent structures in the turbulent pipeflow and the ensuing laminarization process.

NUMERICAL METHOD

A direct numerical simulation (DNS) is performed for flow in an axisymmetric circular pipe with a gradual expansion. OpenFOAM® v. 2.4, an open source computational fluid dynamics software package, is used to solve the incompressible Navier–Stokes equations (Chen et al. 2014; Jasak 1996) through a finite-volume discretization approach. The accuracy of OpenFOAM for DNS of incompressible turbulent flows was investigated by Van Haren (2011) for turbulent channel and pipe flows and Vigolo et al. (2013) for a T-junction geometry.

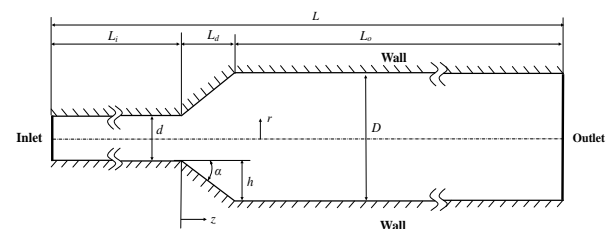


Figure 1: Schematic of the computational domain

Figure 1 illustrates the geometry and computational of the flow through the gradual expansion. As shown, it consists of three main regions: (i) the straight inlet pipe, (ii) the diverging section and (iii) the straight outlet pipe. Simulations are performed for an outlet-to-inlet diameter expansion ratio of $D/d = 2$ and a Reynolds number of 5300

* PhD student

† Assistant professor; corresponding author

based on the diameter and maximum velocity in the inlet pipe. The streamwise lengths of the domain are $L_i = 10d$, $L_d = 1d$, $L_o = 29d$. The divergence angle is $\alpha = 26.57^\circ$. An annular ribbed turbulator of height $0.06d$ is added to the inlet pipe at $5d$ to trigger turbulent flow conditions in the DNS, and the flow at $7.5d$ is periodically recycled back to the inlet boundary allow fully-developed turbulence to develop in the inlet pipe. To keep the desired through-flow mass flux, the average volumetric mass flux of the remapped flow is corrected at each time step (Baba-Ahmadi and Tabor 2009). The location of the mapping plane is far enough from the inlet boundary that the developed turbulence contains multiple instances of the largest eddy length scales (Tabor et al. 2004). As the mapping is conducted over many cycles, it produces fully-developed turbulent flow conditions upstream of the gradual expansion. The resulting turbulence intensity at $2.5d$ upstream of the gradual expansion is approximately $0.055 \bar{U}_{max}$. A no-slip condition is used for radial boundaries, and the outlet boundary condition is zero-gauge static pressure and zero streamwise velocity gradient. Insensitivity of the results to the length of the outlet pipe was examined by repeating the DNS with a domain length of $45d$ with negligible impact on the results.

A structured non-uniform grid consisting of orthogonal finite volumes is mapped to the computational domain illustrated in Figure 1. The grid is refined spatially to have at least three cells within the viscous sublayer which are on the order of the Kolmogorov length scale (η). A mesh convergence is studied using four different block-structured grid resolutions with 1.3 million to 30.4 million cells. The detailed information about the grid cells in the inlet, expansion and outlet is illustrated in Table 1 for each of the simulated cases; N_r , N_θ , and N_z refers to number of cells in the radial, circumferential, and streamwise directions, respectively.

Table 1: Characteristics of computational grids used

Grid Level	$(N_r, N_\theta, N_z)_i$ Upstream of expansion	$(N_r, N_\theta, N_z)_o$ Downstream of expansion	Total cells
G1	(33, 84, 195)	(33, 84, 384)	1,323,651
G2	(49, 128, 293)	(49, 128, 576)	4,554,752
G3	(65, 168, 391)	(65, 168, 768)	10,598,364
G4	(98, 256, 488)	(98, 256, 960)	30,358,016

The governing equations are discretized based on central differencing and second-order Euler backward differencing for the spatial and temporal derivatives, respectively. Water at 1 atm and 25°C is the working fluid. The computational time step size in each case varies according to the resolution of the spatial grid. In order to accommodate start-up effects associated with the imposed initial velocity field, the time-step size is set for each simulation to keep the maximum Courant number less than 0.05 for all cases during the first 1000 iterations (Wu and Moin 2008). The computational time step is then increased such that the maximum Courant number is less than 0.5. Each simulated test case is initialized with a zero relative static pressure and an initial velocity equal to the mean velocity at the inflow boundary and are then integrated in time for approximately 10 flow

through times (defined as $L_i/U_i + L_o/U_o$, where subscripts i and o denote inlet and outlet pipe, respectively) to reach a statistically-steady state, following which approximately four flow through times were collected for analysis. The simulations are partitioned and executed in parallel on 512 processors using a message-passing interface (MPI) parallelization strategy.

INLET TURBULENCE STATISTICS

Validation of the numerical algorithm is accomplished by comparing the turbulent flow in the inlet pipe at a streamwise location of $z/d = -2.5$; the coordinate system fixes $z = 0$ at the start of the expansion. Figure 2 compares the DNS results with statistical properties of turbulent pipe flow available in literature. Figure 2(a) illustrates that the mean turbulent velocity profile agrees well with Wu and Moin (2008), Toonder and Nieuwstadt (1997) and Eggels et al. (1994). Figure 2(b) shows similar agreement in the streamwise fluctuation intensity, u_{rms}^+/u^+ , in the near wall region. Finally, the power spectra of the streamwise velocity fluctuations measured at $r^+ \approx 12$ is shown in Fig. 3. The spectrogram for u , $\psi_{uu}^+ = f/u_\tau^2 \psi_{uu}$ is plotted as a function of the dimensionless frequency, $f^+ = fv/u_\tau^2$, where u_τ is the local friction velocity and ψ_{uu} is the power spectral density of streamwise velocity fluctuations. A spline curve fit of the spectra also plotted (least-squares regression coefficient $R^2 = 0.926$). The trend is very consistent with the experimental results of Toonder and Nieuwstadt (1997). Figures 2-3 confirm the effectiveness of the present approach for resolving the turbulence in the inlet pipe and the suitability of OpenFOAM for the DNS.

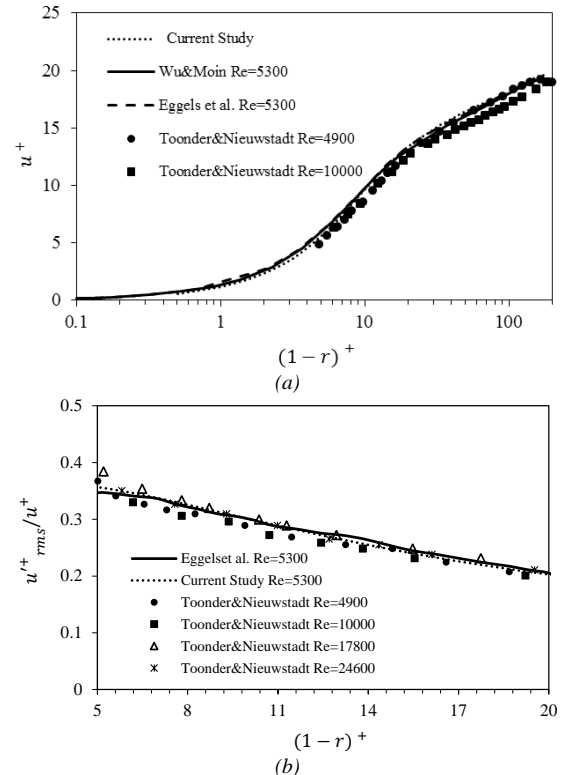


Figure 2: (a) Mean velocity profile and (b) streamwise fluctuation intensity of the turbulence in the inlet pipe

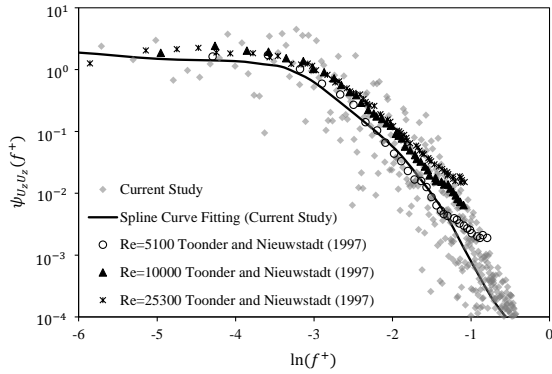


Figure 3: Power spectrum of streamwise velocity fluctuations at $z/d = -2.5$ and $r^+ \approx 12$

RESULTS AND DISCUSSION

In the present discussion of the results, lengths are normalized by the expansion step height, $h = 0.5d$, and velocities are normalized by the maximum average velocity at the inlet, \bar{U}_{max} . The turbulence in the inlet pipe upstream of the expansion is characterized in Figs. 2-3 above. The instantaneous and mean velocity field that occurs downstream of the gradual expansion is shown in Fig. 4(a)-(b). Regions of separated flow exist in the corners near the gradual expansion. As the turbulent core flow in the inlet pipe mixes with the low-momentum flow near the outer wall, transverse momentum transfer causes the centreline velocity to be reduced by approximately half. Figure 4(c) shows that this mixing produces an abrupt increase in the local turbulence kinetic energy (k) near the interface of the core and outer-wall flow that spreads outwards towards the centreline and then decreases as the flow laminarizes due

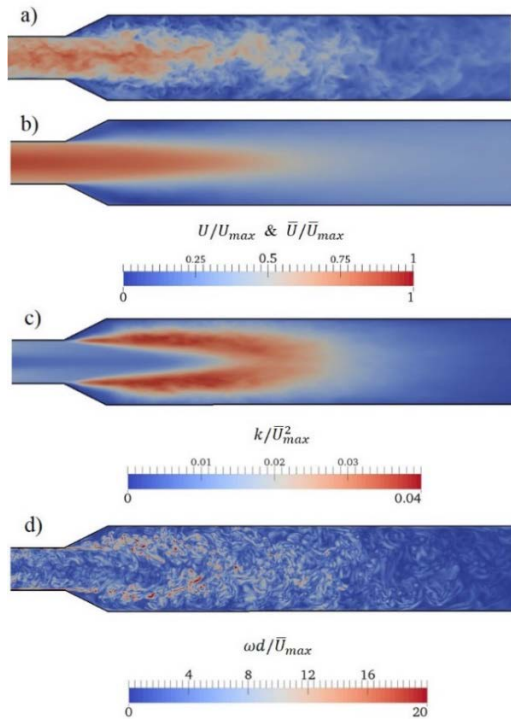


Figure 4: Contours in an axial slice near the gradual expansion; a) instantaneous velocity magnitude, b) mean velocity magnitude, c) turbulence kinetic energy, d) instantaneous vorticity magnitude. (Zoomed view).

to the reduced Reynolds number after the expansion. The associated instantaneous vorticity field in Fig. 4(d) shows that an annular turbulent mixing layer is formed at the sudden expansion, and the roll-up instability of this layer assists in the transverse mixing between the core and outer-wall regions. Larger-scale, coherent vortex structures are initially present in the mixing layer, but gradually lose their coherence as smaller-scale structures are produced more uniformly across the pipe diameter. The streamwise distribution of turbulence kinetic energy along the centreline is plotted in Fig. 6. The location where the small-scale vortex structures uniformly span across the whole outer pipe diameter corresponds to the point with maximum turbulence kinetic energy. Dissipation of the small-scale structures corresponds with the decreasing turbulence kinetic energy in the laminarizing zone.

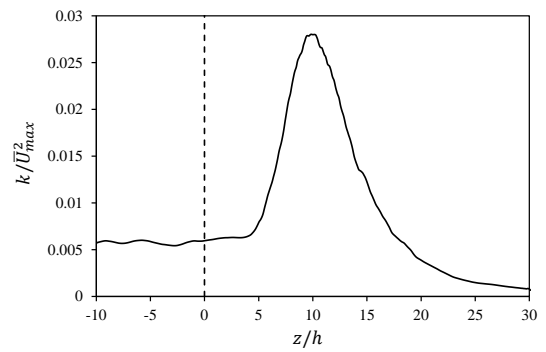


Figure 5: Streamwise distribution of turbulence kinetic energy along the pipe centerline ($r = 0$)

The spatial distribution of the turbulent fluctuations is presented in Fig. 6 through radial profiles of the root-mean-square (rms) of the velocity components at four axial locations. At $z/h = 10$, which corresponds to the maximum turbulence kinetic energy location, the axial fluctuation intensity is approximately 40% larger than the azimuthal and radial components. By $z/h = 22$, which is well into the laminarizing zone, the three components have approximately equal fluctuation intensities, indicating that the flow disturbances become nearly isotropic during relaminarization. It is also notable that the axial and azimuthal disturbances become nearly spatially homogeneous in the laminarizing zone, while the radial disturbances seem to be damped near the wall.

The development of the separated mixing layer and the interaction with the turbulent core flow is studied through budgets of the instantaneous vorticity transport equation (Kundu and Cohen, 2004),

$$\frac{\partial \omega_i}{\partial t} = -(\mathbf{u}_i \cdot \nabla) \omega_j + (\omega_i \cdot \nabla) u_j + \nu \nabla^2 \omega_i. \quad (1)$$

The terms on the right hand side respectively are vorticity convection by the instantaneous velocity field, production via vortex stretching ($i = j$) and tilting ($i \neq j$) mechanisms, and viscous diffusion. The budgets of Eqn. (1) in an axial slice through the centreline are plotted in Fig. 7. The vorticity growth rate in Fig. 7(a) shows that high vorticity growth rate occurs in the turbulent boundary layer of the inlet pipe, which Fig. 7(b) identifies is mainly attributable to convection of vorticity by the turbulent velocity field. This vorticity is convected into the gradual expansion,

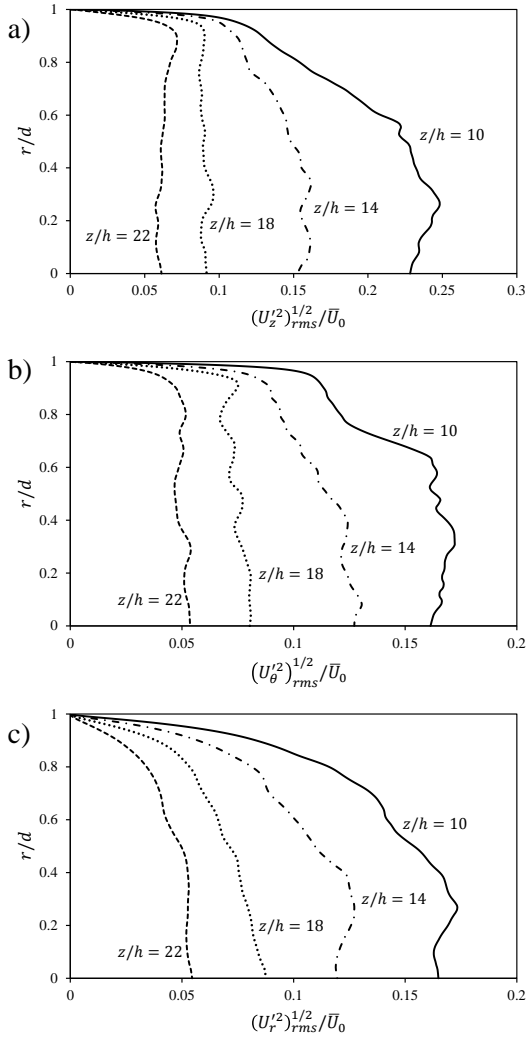


Figure 6: Radial profiles of the root-mean-square velocity fluctuations at various axial locations

where Fig. 7(c) shows that vorticity production mechanisms are activated and enhance the production of vorticity within and immediately downstream of the sudden expansion. Vorticity production is localized primarily in the region where the inlet-pipe core flow interacts with the separated mixing layer. Viscous diffusion of vorticity is plotted in Fig. 7(d), which shows that viscous diffusion is largest in the near-wall region in the inlet pipe, where the mean vorticity gradient (i.e. mean shear) is highest. Downstream of the expansion, the mean shear reduces owing to the reduced Reynolds number. As a result, the viscous diffusion of the vorticity moves away from the wall nearer to the centerline.

Figure 8 plots the relative magnitude of the vortex stretching and tilting mechanisms of the vorticity production term in Eqn. (1). The contours show the magnitude of the relative terms normalized by $(\bar{U}_{max}/d)^2$. Again, the interaction between the inlet-pipe core flow and the separated mixing layer is noted to significantly increase the overall vorticity production rate, shown in Fig. 8(a). When broken into the stretching and tilting mechanisms shown in Fig. 8(b) and (c), respectively, the two

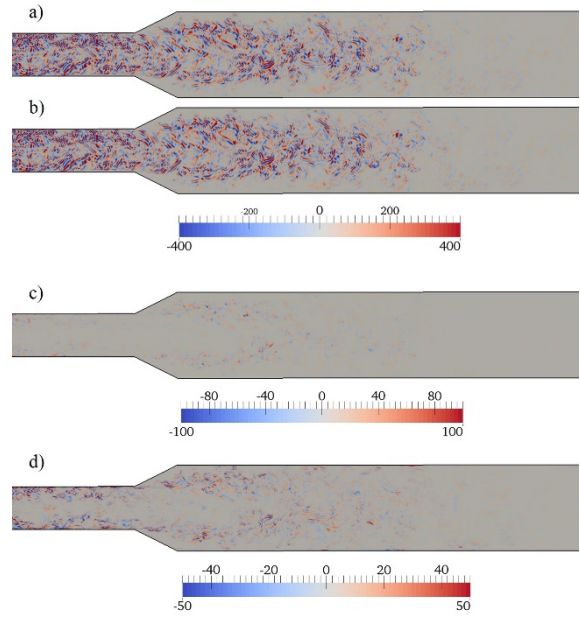


Figure 7: Contour levels of the budgets of instantaneous vorticity transport terms: a) vorticity growth rate, b) vorticity convection term, c) vorticity production term, d) vorticity diffusion rate.

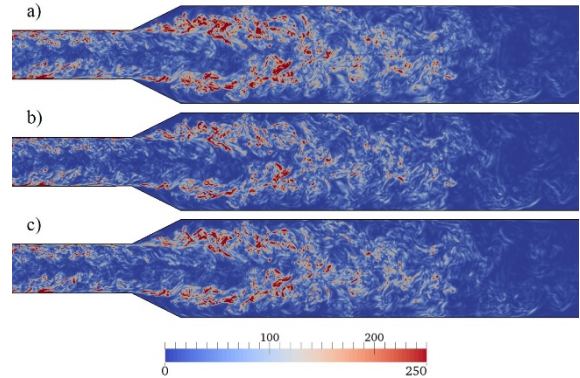


Figure 8: Contours illustrating the magnitude of the vorticity production rate from Eqn. (1): (a) overall production rate, (b) stretching mechanism, (c) tilting mechanism. Contours are normalized by $(\bar{U}_{max}/d)^2$.

mechanisms seem to have roughly equivalent contributions to the production of vorticity in the flow.

The spatial evolution of the vorticity production and diffusion budgets are plotted in Fig. 9 through contours at four axial slices. Vorticity production and diffusion rates are highest near the separated mixing layer. Upstream of $z/h = 2$ (not shown), the production and dissipation rate contours are relatively contiguous in the azimuthal direction. However, by $z/h = 2$, the budgets are grouped into coherent regions. This indicates that inviscid instability modes have been activated in the mixing layer that produced roll-up into azimuthally-spaced coherent vortical structures. Figure 8 also supports such a conclusion; roll-up of the contiguous mixing layer into axially-spaced vertical structures is also visible immediately downstream of the sudden expansion. The azimuthal coherence of vorticity budgets within the mixing layer continuous to degrade

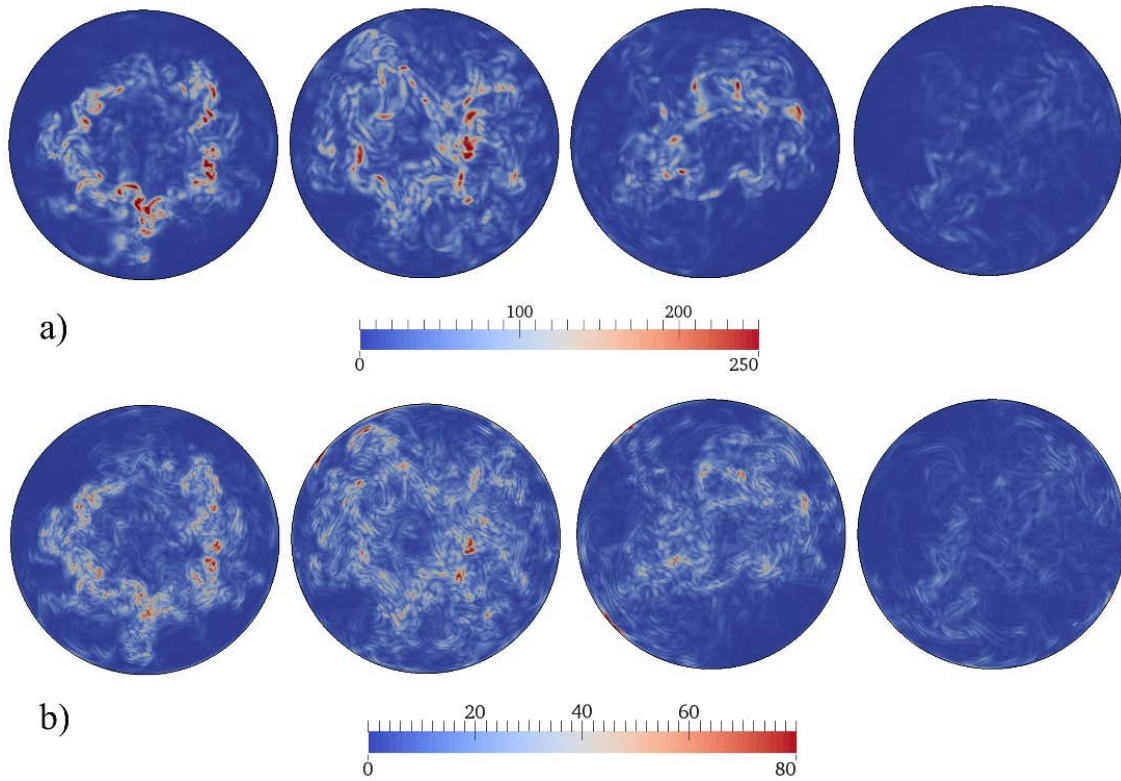


Figure 9: Contours of the budgets of instantaneous vorticity (a) production (b) diffusion rate terms. Axial locations are (from left to right) $z/h = 2, 6, 10, 14$.



Figure 3: Instantaneous vortical structures visualized by iso-surfaces of the second invariant of the velocity gradient tensor, $Qd/U_0 = 4.7$ (Zoomed view).

downstream of $z/h = 2$ as the coherent vortical structures are broken into small-scale structures in the laminarizing zone. The structure of the coherent vortices is visualized in Fig. 10 by iso-surfaces of the second invariant of the velocity gradient tensor normalized by U_0/d . The appearance of coherent vortical structures depends on the threshold value of iso-surfaces. As observed, the vortical clusters are oriented in both streamwise and spanwise directions, forming prograde and retrograde hairpin vortices. Downstream of the gradual expansion, the vortical clusters are reoriented more in the spanwise direction and gradually disappear due to laminarization of the flow.

CONCLUSIONS

Turbulent pipe flow at an inlet Reynolds number of 5600 through a 26.57° gradual expansion with an expansion ratio of 2:1 is investigated using direct numerical simulation in OpenFOAM®. Turbulence in the inlet pipe with an intensity of 5.5% is developed using a ribbed

turbulator and a streamwise-periodic remapping procedure. The simulated turbulence in the inlet pipe is validated against numerical and experimental results for pipe flows at similar Reynolds numbers, achieving excellent agreement in terms of the mean velocity profile, fluctuation amplitudes, and spectral content. A turbulent mixing layer is formed immediately downstream of the gradual expansion as the inlet-pipe core flow separates from the outer wall. Transverse momentum exchange between the high-speed turbulent core and the separated outer-wall flow is facilitated by the instability of the mixing layer via inviscid modes. Analysis of the budgets of the instantaneous vorticity transport equation illustrates that this instability results in the roll-up of the mixing layer into hairpin-shaped coherent vortical structures. The orientation of the hairpin vortices are both prograde (legs pointing upstream) and retrograde (legs pointing downstream). These structures trigger vorticity production and diffusion mechanisms that result in the rapid growth in vorticity inside and immediately downstream of the sudden

expansion. As the structures are broken into relatively spatially-uniform, small-scale vortices, the point where the vortex scales are most uniform across the diameter of the pipe corresponds to the location of maximum turbulence kinetic energy and maximum anisotropy of the turbulent fluctuations. Downstream of this location, diffusion of vorticity and turbulence dissipation results in a gradual laminarization of the flow and progression towards more spatially homogeneous and isotropic velocity fluctuations in the laminarized region of the outlet pipe.

REFERENCES

- Baba-Ahmadi, M. H., and G. Tabor, 2009. "Inlet Conditions for LES Using Mapping and Feedback Control." *Computers and Fluids* 38 (6). Elsevier Ltd: 1299–1311. doi:10.1016/j.compfluid.2009.02.001.
- Chen, G., Q. Xiong, P.J. Morris, E.G. Paterson, A. Sergeev, and Y. Wang, 2014. "OpenFOAM for Computational Fluid Dynamics." *Notices of the AMS* 61 (4): 354–63.
- den Toonder, J. M. J., and F. T. M. Nieuwstadt, 1997. "Reynolds Number Effects in a Turbulent Pipe Flow for Low to Moderate Re." *Physics of Fluids* 9 (11): 3398. doi:10.1063/1.869451.
- Duguet, Y, 2015. "Pipe Flow Clogged with Turbulence." *Journal of Fluid Mechanics* 776: 1–4. doi:10.1017/jfm.2015.285.
- Eggels, J. G. M., F. Unger, M. H. Weiss, J. Westerweel, R. J. Adrian, R. Friedrich, and F. T. M. Nieuwstadt, 1994. "Fully Developed Turbulent Pipe Flow: A Comparison between Direct Numerical Simulation and Experiment." *Journal of Fluid Mechanics* 268 (1): 175. doi:10.1017/S002211209400131X.
- Jasak, H, 1996. "Error Analysis and Estimation for the Finite Volume Method with Applications to Fluid Flows, 1996." Ph. D. Thesis, Imperial College.
- Kundu, P.K. and I. M. Cohen, 2004. "Fluid Mechanics." 3rd ed, Elsevier Academic Press.
- Moallemi, N., and J.R. Brinkerhoff, 2016. "Numerical Analysis of Laminar and Transitional Flow in a Planar Sudden Expansion." *Computers & Fluids* 140: 209–21. doi:10.1016/j.compfluid.2016.10.003.
- Moallemi, N. and J.R. Brinkerhoff, 2016. "Generation of Turbulent Inflow Conditions for Pipe Flow via an Annular Ribbed Turbulator." In *69th Annual Meeting of the APS Division of Fluid Dynamics*. Portland, Oregon.
- Peixinho, J., and H. Besnard, 2013. "Transition to Turbulence in Slowly Divergent Pipe Flow." *Physics of Fluids* 25 (11). doi:10.1063/1.4833436.
- Selvam, K., J. Peixinho, and A.P. Willis, 2015. "Localised Turbulence in a Circular Pipe Flow with Gradual Expansion." *Journal of Fluid Mechanics* 771: 1–13. doi:10.1017/jfm.2015.207.
- Tabor, G.R., M. H. Baba-Ahmadi, E. de Villiers, and H.G. Weller, 2004. "Construction of Inlet Conditions for LES of a Turbulent Channel Flow." *Proceedings of the European Conference on Computational Fluid Dynamics*, no. January: 1–12.
- Van Haren, S W, 2011. "Testing DNS Capability of OpenFOAM and STAR-CCM." Master Thesis, University of Delft.
- Vigolo, D., I. M. Griffiths, S. Radl, and H. A. Stone, 2013. "An Experimental and Theoretical Investigation of Particle-wall Impacts in a T-Junction." *Journal of Fluid Mechanics* 727: 236–55. doi:10.1017/jfm.2013.200.
- Wu, X., and P. Moin, 2008. "A Direct Numerical Simulation Study on the Mean Velocity Characteristics in Turbulent Pipe Flow." *Journal of Fluid Mechanics*. Vol. 608. doi:10.1017/S0022112008002085.